RSC Sustainability

ROYAL SOCIETY OF CHEMISTRY

PAPER

View Article Online
View Journal | View Issue

Cite this: *RSC Sustainability*, 2026, **4**, 1527

Design of fully reprocessable composite non-isocyanate polyurethane (NIPU) foams from sustainable blends of cyclic carbonates

Federica Orabona, †[ab] Federica Recupido,†[c] Krzysztof Polaczek,[c] Giuseppe Cesare Lama,[c] Martina Morra,[b] Francesco Taddeo,[b] Martino Di Serio,[b] Tapio Salmi,[ab] Letizia Verdolotti *[c] and Vincenzo Russo[ab]

In response to the growing need to reduce reliance on petrochemical feedstock and eliminate toxic isocyanates in polyurethane production, this study presents the synthesis of composite non-isocyanate polyurethane (NIPU) foams starting from a novel blend of bio-based cyclic carbonates. The resulting flexible foams are fully reprocessable and have a bio-based content ranging from 92% to 99%. They were prepared through a two-step procedure where aminolysis was first carried out between 1,4-butane diamine (BDA) and blends of carbonated soybean oil (CSBO) and bio-based butanediol bis-cyclic carbonate (BCC). A blowing reaction was induced *via* *S*-alkylation using a dithiol while diatomite was incorporated as a renewable nanoporous filler providing nucleating and reinforcing properties. The influence of the CSBO/BCC ratio on foam properties was systematically investigated through chemical, physical, thermal, and morphological analyses. A structure–property relationship was established using an adapted Gibson–Ashby model. The resulting foams exhibited open-cell morphology with uniform cell sizes (400–600 μm) and apparent densities between 200 and 250 kg m^{-3}. Notably, the foams were successfully re-shaped into flexible films *via* temperature-controlled compression molding, confirming their potential for recyclability and reuse. The stress-relaxation behavior of the re-processed NIPU presented a decreasing trend by increasing the relaxation time and was described by the Kohlrausch–Williams–Watts function. The activation energy was calculated according to the Arrhenius equation and was found to be 91 ± 8 kJ mol^{-1} indicating a relatively strong temperature dependence of the relaxation mechanisms. This work unlocks a new design strategy for the sustainable synthesis of fully recyclable NIPU foams, opening up new directions in green polyurethane chemistry.

Received 23rd December 2025
Accepted 23rd January 2026

DOI: 10.1039/d5su00946d

rsc.li/rscsus

Sustainability spotlight

This work advances bio-based non-isocyanate polyurethane (NIPU) foams derived primarily from renewable resources such as carbonated soybean oil, achieving a bio-based content up to 99%. By eliminating toxic isocyanates, these materials would promote good health and well-being of both manufacturers and end-users in line with the United Nations Sustainable Development Goal (SDG) 3. The use of renewable feedstocks and highly bio-based formulations supports responsible consumption and production (SDG 12), while reducing dependence on fossil resources and associated impacts on the ecosystem, as well as the need for land-intensive fossil fuel extraction processes (SDG 15). By enabling the replacement of conventional petrochemical polyurethane systems with renewable and reprocessable alternatives, this research contributes to the strategies to mitigate climate change (SDG 13).

1. Introduction

Polyurethane (PU) foams are among the most widely used polymeric material classes with an annual production of approximately 20 million metric tonnes.[1,2] PU foams can be either flexible or rigid materials and, thanks to their versatility, they can be utilized in many different sectors. Flexible foams, characterized by open and interconnected cell morphology, are mainly employed in the production of mattresses, automotive or aerospace components, furniture,[3,4] or in acoustic/shock insulation applications.[5] Conversely, rigid foams, consisting of closed-cell structures, are used mainly as thermal insulation materials in the building sector,[6,7] as well as in automotive and transport applications.[8,9] PU foams are synthesized through the polyaddition of isocyanates (characterized by NCO groups) and polyols (having OH groups) to attain urethane bonds (NCOOR),

[a]*Johan Gadolin Process Chemistry Center (PCC), Laboratory of Industrial Chemistry and Reaction Engineering (TKR), Åbo Akademi University, Henriksgatan 2, FI-20500, Turku/Åbo, Finland. E-mail: v.russo@unina.it*

[b]*Chemical Sciences Department, University of Naples Federico II, Via Cintia 26, 80126 Naples, Italy*

[c]*National Research Council, Institute for Polymers, Composites and Biomaterials, 80055, Portici, Naples, Italy. E-mail: letizia.verdolotti@cnr.it*

† These authors equally contributed to this work.

followed by a blowing process,[10] which can be conducted with the aid of physical blowing agents (BAs), *i.e.*, low-boiling point chemicals, or through chemical reactions between isocyanates and chemical BAs releasing CO_2 *in situ*. In both cases, the resulting gases are entrapped in the polymeric matrix leading to its expansion.[1,11]

However, PU precursors are typically derived from petrol-based sources. Moreover, isocyanates are derived from extremely poisonous phosgene and are classified as Carcinogenic, Mutagenic, and Reprotoxic (CMR), being gradually limited or in some cases even banned by the European Union.[12–14] Therefore, the major focus has been on the development of isocyanate-free routes with aminolysis of 5-membered cyclic carbonates (CCs) with diamines being the most promising at present. Polyhydroxyurethane (PHU) linkages with different pending primary and secondary OH groups are formed,[15–17] which corresponds to intriguing molecular structures with enhanced reprocessing characteristics. Both CCs and diamines can be obtained from renewable building blocks.[18,19] CCs can be synthesized by cycloaddition of CO_2 to epoxides[20–24] derived from renewable sources such as vegetable oils,[25–29] terpenes, *e.g.*, limonene, cholesterol[16,29,30] and sugars/carbohydrates,[16,29,31] while aliphatic and aromatic diamines can be synthesized from fermentation of sugars.[32,33] However, the polyaddition reaction between CCs and diamines is typically slower than the traditional isocyanate-based route, due to the lower reactivity of CCs and steric hindrance limitations.[34,35] Although aminolysis can proceed without catalysts and under mild conditions,[36,37] its kinetics is usually enhanced by organocatalysts, such as 1,8-diazabicyclo[5.4.0]undec-7-ene (DBU),[34] 1,5,7-triazabicyclo[4.4.0]dec-5-ene (TBD)[15] and 1,4-diazabicyclo[2.2.2]octane (DABCO),[38] at 80–120 °C for 1–14 h. To produce NIPU foams, different blowing approaches have been reported involving physical BAs, such as hydrofluorocarbons (Solkane 365/227)[38] and supercritical CO_2,[39] as well as chemical BAs such as sodium bicarbonate.[40] The resulting processes are known as non-self-blowing routes. New strategies have been explored for synthesizing self-blowing NIPU foams using suitable chemical BAs which react with the monomers releasing the blowing gas *in situ* and at the same time take part to the final polymer network.[18] Typical BAs for self-blowing NIPUs are siloxanes,[15,36,41] thiols[34,42–46] and water.[47] These agents react either with diamines to generate hydrogen gas (H_2) or with CCs to produce CO_2 through decarboxylation triggered by thermal routes[31] or organocatalysts.[18] Recently, Monie *et al.* introduced the possibility of using thiols[42] and thiol derivatives[34] to decarboxylate CCs *via* *S*-alkylation. It consists of the nucleophilic attack of thiols on cyclic carbonates, leading to the formation of hydroxythioether linkages and CO_2. The resulting polymers are named as non-isocyanate polyhydroxyurethane (NIPHU) foams, where hydroxyurethane units alternate with hydroxythioether ones along the polymer chains.[42] *S*-Alkylation of cyclic carbonates is not only advantageous because it produces the blowing gas *in situ*, but also because the thiol takes part in the final polymer backbone providing enhanced properties to the final material, such as a higher thermal stability[42,43] and easier reprocessability.[43–45] As a matter of fact, the presence of OH groups along the polymer chains enables dynamic exchange reactions such as reversible urethane bond formation and transcarbamoylation reactions.[46]

Despite the high potential of the *S*-alkylation route in the synthesis of self-blowing NIPU foams, it remains largely unexplored when fully bio-based bulky substrates such as vegetable oil based-CCs[43,48] are utilized. For instance, carbonated soybean oil (CSBO), derived from one of the most abundant vegetable oils, has only been employed to produce compact NIPU materials such as coatings, elastomers, and nanocomposites,[28,49–51] and for the synthesis of NIPU foams in non-self-blowing formulations, *i.e.*, by utilizing azodicarbonamide/zinc oxide (AZO/ZnO)[25] and ammonium bicarbonate/citric acid mixtures[48] as blowing agents. Similarly, butanediol bis-cyclic carbonate (BCC), obtained from the carbonation of butanediol diglycidyl ether, has been previously reported for the synthesis of compact NIPU materials,[52,53] and only in one case in the synthesis of NIPU foams.[44] Apart from the use of individual CCs, the combination of bio-based CCs with complementary functionality has been scarcely investigated, despite its strong potential in tailoring key properties of NIPU foams, including cellular morphology, mechanical strength, and functional performance.

In this context, the present work focuses on the valorization of bio-based cyclic carbonate blends for the synthesis of self-blowing composite NIPU foams *via* the *S*-alkylation approach by precise formulation design. For the first time, CSBO and BCC are combined as complementary precursors in the aminolysis reaction with bio-based 1,4-butane diamine (BDA) catalyzed by DBU. *S*-Alkylation with 3,6-dioxa-1,8-octanedithiol (DODT) was selected as the blowing reaction. The incorporation of silica-based nanofillers in PU formulations has already been demonstrated to promote morphological uniformity and insulation properties.[54] In this case, for the first time, diatomite derived from the siliceous fossilized skeletons of diatoms has been used as a renewable nucleating agent[6,55,56] for NIPU foams. Foam properties were tuned by varying the CSBO/BCC ratio and comprehensively characterized through thermal, chemical, mechanical, and morphological analyses. Dedicated experiments were carried out to elucidate the *S*-alkylation dynamics of CSBO and BCC using quantitative FTIR analysis. To correlate foam morphology with mechanical properties, an adapted Gibson–Ashby model was applied.[11] Additionally, the reprocessability of NIPU foams self-blown into new materials was assessed *via* compression molding. The dynamic behavior of the reprocessed materials was subsequently investigated through stress-relaxation experiments and quantitatively analyzed using the Kohlrausch–Williams–Watts (KWW) and Arrhenius models.[43]

Overall, this work provides a new formulation platform for designing fully bio-based, reprocessable NIPU composite foams. This strategy not only enables tailored properties of the final materials but also provides new perspectives for replacing conventional PU foams in diverse application sectors. Furthermore, the demonstrated reprocessing of NIPU foams into second-generation materials highlights their circularity and supports their future scalability as sustainable alternatives.

2. Experimental section

2.1 Materials and reagents

Epoxidized soybean oil (ESBO, epoxy group concentration of 4.43 mol L^{-1}) was provided by Kchimica (Mirano, Italy). Tetrabutylammonium bromide (TBAB) and ethyl acetate were supplied by Sigma-Aldrich (Milan, Italy). 1,4-Diaminobutane (BDA, purity >98%, M_w = 88.15 g mol^{-1}), 3,6-dioxa-1,8-octanedithiol (DODT, M_w = 182.3 g mol^{-1}, f = 2), and the polymerization/*S*-alkylation catalyst 1,8-diazabicyclo(5.4.0) undec-7-ene (DBU) were provided by Tokyo Chemicals Industry (Tokyo, Japan). The filter agent, Diatomite Celite® 545, selected as a nucleating agent, was supplied by Sigma-Aldrich (Milan, Italy). 4,4′-[1,4-Butanediylbis(oxymethylene)]bis[1,3-dioxolan-2-one], butanediol bis(cyclocarbonate) (BCC, SP-68-021, f = 2, molecular weight, M_w = 290.27 g mol^{-1}) was kindly provided by Specific Polymers (Castres, France). Deuterated chloroform ($CDCl_3$, M_w = 120.4 g mol^{-1}, 99.8 atom % D), employed as a solvent for ^{1}H-NMR spectroscopy, and tetrahydrofurane (THF) (anhydrous, 99.9% purity) were purchased from Sigma-Aldrich (Milan, Italy). All the chemicals were used as received.

2.2 Synthesis of carbonated soybean oil (CSBO)

The cycloaddition of CO_2 to ESBO (Scheme 1) was carried out in a 300 mL stainless-steel Parr batch reactor equipped with a gas-entrainment impeller and heating jacket (Fig. S1, Section S1, SI). The temperature of the gaseous and liquid phases was controlled using two thermocouples, while the pressure was controlled using a manometer connected to a Picolog online data acquisition system. Characterization of the ESBO before the carbonation experiments was performed by Gas Chromatography-Mass Spectroscopy (GC-MS), titration of epoxy groups, and ^{1}H-NMR (Section S1, SI).

In a typical carbonation experiment, 100 g of ESBO and 7.5 g of TBAB were charged to the system and the temperature was set at 130 °C while the stirring rate was adjusted at 800 rpm, following the procedure outlined in the literature.[57] Before switching to the CO_2 flow, the lines to the reactor were cleaned with N_2, then CO_2 was continuously fed into the system at 40 bar for 24 h to ensure complete conversion of ESBO to the carbonated product (CSBO). Samples were withdrawn during the experiment and analyzed *via* both ^{1}H-NMR (500 MHz) and titration of the epoxy groups through the protocol reported by Jay *et al.*[58] Subsequently, TBAB was separated from the reaction mixture through 5 cycles of solvent extraction with ethyl acetate and water in a separation funnel. Finally, ethyl acetate and traces of water were evaporated in a rotavapor at 65 °C, 100 mbar, and 50 rpm for 1 h. The separation was checked by ^{1}H-NMR from the disappearance of the signal at 3.3 ppm. The final product was fully characterized by ^{1}H-NMR and Fourier transform infrared (FTIR) spectroscopy.

2.3 *S*-Alkylation dynamic experiments

S-Alkylation of CCs with DODT was selected as the self-blowing route, causing the ring-opening of the CCs and releasing CO_2 *in situ*. Prior to the synthesis of NIPU foams, dedicated experiments were focused on the reactivity of the CCs with DODT. Specifically, a solution of CSBO/DODT in a 1 : 1 ratio was reacted for 120 min at 120 °C with 10 mol% DBU. Samples were collected in 20 min intervals and analyzed *via* Attenuated Total Reflectance-Fourier Transform Infra-Red (ATR-FTIR) spectroscopy at room temperature. The same experiment was repeated with BCC and DODT in a 1 : 1 ratio. The CC conversion over time (eqn (1)) was quantitatively determined by integrating the peak of the CCs at 1800 cm^{-1}, after deconvolution with the Lorentz function using Origin software (v. 16, Origin Lab, Northampton, MA, USA).

$$\text{Conversion} = \frac{R_{CC,t_0} - R_{CC,t}}{R_{CC,t_0}} \times 100 \quad (1)$$

$$R_{CC,t} = \frac{A_{CC,t}}{A_{ref}} \quad (2)$$

where $R_{CC,t}$ and R_{CC,t_0} (eqn (2)) are the ratios between the area of the peak at 1800 cm^{-1} ($A_{CC,t}$) at a specific reaction time t and time zero, respectively, and the reference area (A_{ref}), *i.e.*, the area of the peaks at 3000 cm^{-1} corresponding to stretching of C–H groups.[21]

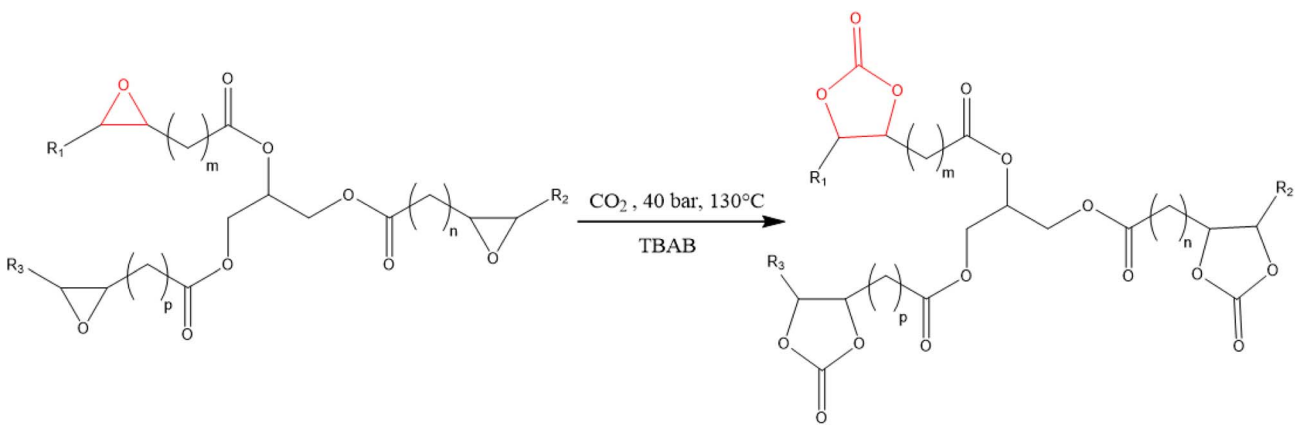

Scheme 1 CO_2 cycloaddition to epoxidized soybean oil (ESBO) to get carbonated soybean oil (simplified scheme).

2.4 Synthesis of NIPU foams

The composite NIPU foams were synthesized using the precursors and additives shown in Fig. 1a through a two-step process schematized in Fig. 1b: (i) pre-polymerization *via* aminolysis and (ii) foaming *via S*-alkylation (based on Pearson's hard–soft acid–base theory).[59] In the first step, CSBO (or the CSBO-BCC blend) was preheated in an oven at 60 °C with BDA for 15 min to reduce the viscosity. 1.5 wt% diatomite (previously

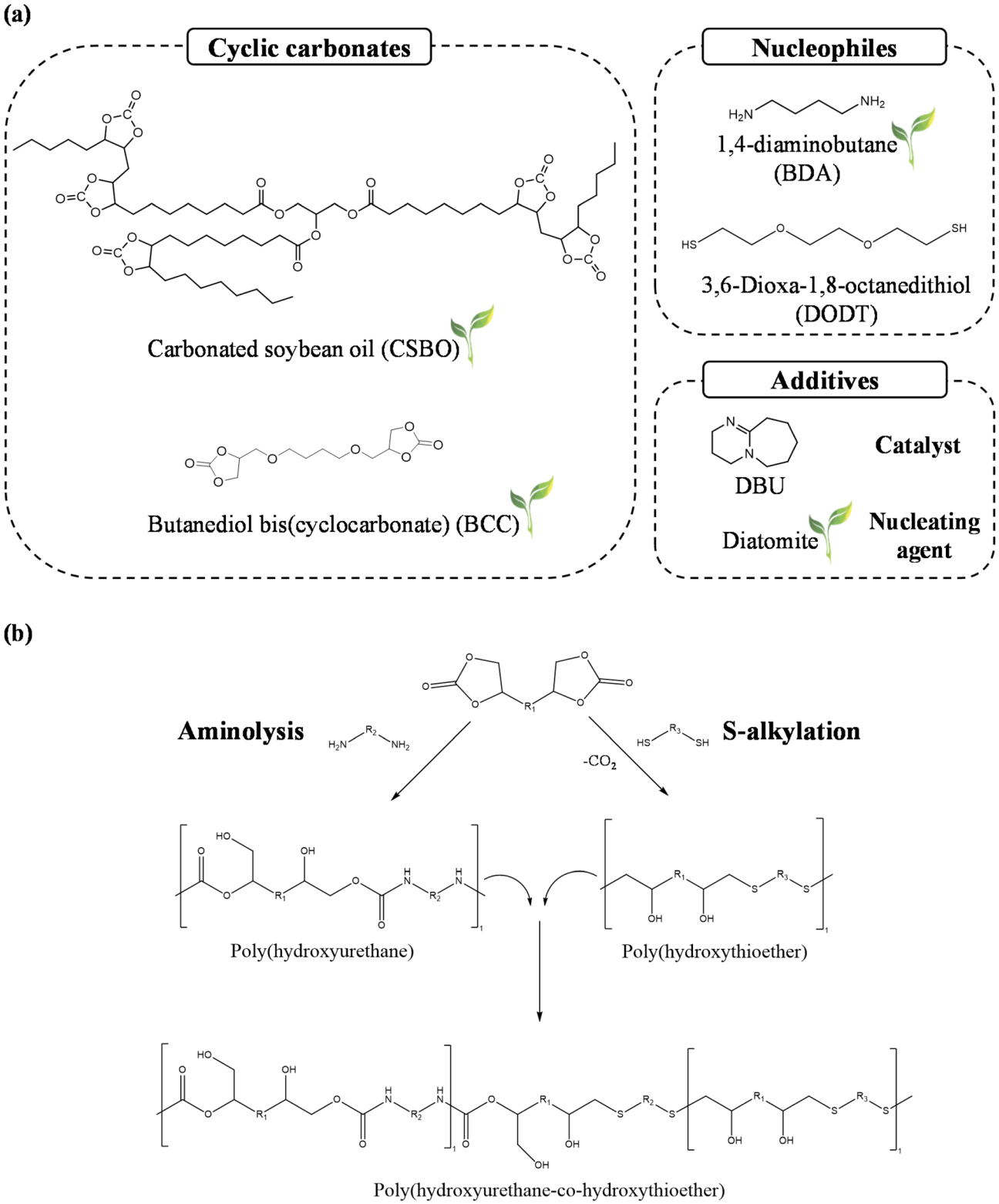

Fig. 1 (a) Molecular structures of the precursors and additives employed. (b) Aminolysis of CCs with diamines (first step) and *S*-alkylation between CCs and thiols (second step), resulting in the formation of poly-hydroxyurethane and poly-hydroxythioether linkages.

Table 1 Experimental conditions of foam synthesis

Sample name	CC type	Pre-foaming time (min)	CSBO : BCC : BDA : DODT (mol)	DBU (mol% to CC)	Diatomite (wt%)	Bio-content[a] (%)
NIPU_1	CSBO	15	1 : 0 : 0.75 : 0.25	10	1.5	92
NIPU_2	CSBO	15	1 : 0 : 1 : 0	10	1.5	99
NIPU_3	CSBO-BCC	15	0.75 : 0.25 : 0.75 : 0.25	10	1.5	92
NIPU_4	CSBO-BCC	15	0.75 : 0.35 : 0.75 : 0.25	10	1.5	92

[a] Bio-content estimated according to eqn (3).

dried at 80 °C overnight to remove water content) was added, and the mixture was stirred at 450 rpm and 60 °C for 1 min.[41] Next, a DBU catalyst (10 mol% relative to the CSBO or CSBO-BCC blend) was added, and stirring was prolonged for 10 min. In the second step, the *S*-alkylation was performed by adding DODT to the reaction mixture and increasing the stirring rate to 900 rpm for 2 min. Finally, the mixture was poured into a silicone square mold (48 × 48 × 48 mm^3) and cured in an oven at 100 °C for 2 h. Experiments were performed employing different CC compositions and reactant molar ratios as summarized in Table 1. The bio-based content of foams was calculated as the ratio between the mass of the bio-sources derived reactants (w_{bio}) and the total weight (w_{tot}),[6] according to eqn (3).

$$\text{Bio content} = \frac{w_{bio}}{w_{tot}} \times 100 \quad (3)$$

2.5 Re-processability of NIPU foams into new materials

Foams were reprocessed under compression molding in a custom-made stainless-steel two-plate press of cylindrical shape (inner and outer diameters of 48 mm and 80 mm, respectively). Foams were milled into small scraps and placed on a Teflon film in the lower mold plate. The upper plate covered the material, and the press was firmly sealed by applying a total pressure of approximately 2.7 MPa. The system was placed in an oven at 140 °C for 2 h and then gradually cooled down to room temperature.

2.6 Characterization of the precursors and NIPU materials

2.6.1 Epoxy content determination of ESBO. The epoxy content of ESBO was measured *via* both oxirane group titration, according to Jay's method,[58] and ^{1}H-NMR (500 MHz) (Bruker AV500A) by dissolving the samples in $CDCl_3$. ^{1}H-NMR (500 MHz) was also employed to quantitatively determine the yield of CSBO and any by-products.

2.6.2 Chemical analysis. The chemical structures of the precursors, foams and the reprocessed materials were investigated by ATR-FTIR spectroscopy (PerkinElmer Spectrum Frontier Dual Range MIR-NIR instrument). The spectra were collected at room temperature from 4000 cm^{-1} to 500 cm^{-1} with a resolution of 4 cm^{-1}. For the synthesized CC, the bands at 1800 cm^{-1} associated with CSBO formation and at 815–950 cm^{-1} related to the consumption of ESBO were identified.[48]

2.6.3 Thermal analysis. The thermal stability of the selected precursors (CCs and di-thiol) and foams was assessed through thermogravimetric analysis (TGA) and derivative thermogravimetric analysis (DTGA) (TA Q5000, TA Instruments, Water Corporation, New Castle, DE, USA) by imposing a ramp of 10 °C min^{-1} from 30 °C to 600 °C under a N_2 flow (volumetric flow rate = 40 mL min^{-1}). Differential Scanning Calorimetry (DSC, DSC Discovery 2000, TA instruments) was employed to analyze the glass transition temperature (T_g) of the foams and reprocessed materials. Experiments were carried out using three scans imposing a scanning rate of 10 °C min^{-1} under nitrogen flow (50 mL min^{-1}): (i) heating from −80 °C to 140 °C, (ii) cooling from 140 °C to −80 °C and (iii) heating from −80 °C to 200 °C. T_g was determined at the third scan (*i.e.* second heating scan), whereas the first two cycles were intended to remove the thermal history of the materials.

2.6.4 Morphological analysis. The morphological characteristics of NIPU foams were examined through Scanning Electron Microscopy (SEM, SEM Quanta FEI 300, Eindhoven, the Netherlands) at different magnifications using an acceleration voltage of 20 kV. Specimens (0.5 cm × 0.5 cm × 0.5 cm) were cut along the direction perpendicular to the foam growth and sputter-coated with a thin layer of gold/palladium before being analyzed. Image analysis was carried out using customized software (Image Pro Plus 6.1, Media Cybernetics, MD, USA) to quantify specific morphological parameters such as average cell size (D_h, μm), cell size distribution, cell density (N, cm^{-3}) and the anisotropy coefficient (−). The cell density was calculated according to eqn (4).[9]

$$N = \left(\frac{n}{A}\right)^{3/2} \quad (4)$$

where n is the number of cells and A is the area of the acquired SEM image (cm^2). The anisotropy coefficient was estimated as the ratio between the cell width and length. The measurements were conducted considering approximately 100 independent cells.

2.6.5 Apparent density evaluation and mechanical analysis. The apparent density of the foams was obtained by measuring the volume with a micrometer and the weight with an analytical balance (Pioneer OHAUS, Germany). The measurement of the foam core was done in triplicate by removing the outer skin.

The compressive properties of NIPU foams were estimated by Dynamic Mechanical Analysis (DMA, TAQ800 instrument, Water Corporation, New Castle, DE, USA) applying a force of 18 N at 0.5 N min^{-1} at 35 °C. The elastic modulus E' (kPa) was estimated from the stress *vs.* strain curves as the slope of the

tangent to the stress *vs.* strain curves, and the stress at 10% deformation (σ_{10}) was calculated. The specific modulus ($E'^* = E'/\rho$, kPa kg^{-1} m^{-3}) and the specific strength ($\sigma^*_{10} = \sigma_{10}/\rho$, kPa kg^{-1} m^{-3}) were calculated as the normalization of the elastic modulus and compressive strength with respect to the foam density. The experimental data were expressed as the average and standard deviation of three independent measurements.

A more general expression of the Gibson–Ashby model (eqn (5)) with a non-integer exponent n was utilized to describe the mechanical behavior of the examined NIPU foams during the compression tests in a less idealized approach, *i.e.*, considering irregular cell shapes and closed–open hybrid cell morphologies.[60]

$$\frac{E}{E_S} = C\phi^2\left(\frac{\rho}{\rho_S}\right)^n + C'(1-\phi)\left(\frac{\rho}{\rho_S}\right) \quad (5)$$

where C and C' are proportional constants, E/E_S is the relative modulus and ρ/ρ_S is the relative density. The parameter φ is the volume ratio of the solid material constituting the cell edges and ranges from 1 for open cell foams to 0 for closed cell ones, whereas $(1-\phi)$ is the volume ratio of the material constituting the cell walls. E_S and ρ_S are usually the modulus and density of the solid non-porous material taken as a reference,[61,62] which, in this case, corresponded to the compact material obtained from foam reprocessing.[61] The coefficients C and C' were determined by imposing $n = 2$ in eqn (5) and considering the two limiting cases as boundary conditions *i.e.*, $\varphi = 1$ (fully open-cell behavior) to obtain C, and $\varphi = 0$ (fully closed-cell behavior) to obtain C'. Then, these values were substituted in eqn (5), and the parameters n and φ were fitted by nonlinear regression performed through iterative minimization of the objective function between the experimental and modelled values of E/E_S.

The tensile properties of NIPU films obtained from foam reprocessing were analyzed according to the ASTM D 1708-02 standard, in a universal testing machine (model CMT4304 from Shenzhen SANS Testing Machine Co, China), equipped with a 5 kN load cell. Specimens of 6 mm length and 2 mm width (with a thickness in the range of 100–200 μm) were analyzed. Experiments were performed imposing a velocity of 20 mm min^{-1} at 25 ± 2 °C and RH = 50 ± 5%. The tensile strength at maximum deformation (σ_{max}, MPa) and the maximum deformation (ε_{max}, mm) as well as the tensile elastic modulus (E) were calculated from stress–strain curves.

Additionally, DMA analysis (TA Instruments DMA850 equipped with a cooling unit) was selected to measure the tensile storage modulus (E'), tensile loss modulus (E''), and the damping ratio ($\tan\delta = E''/E'$) of the NIPU films obtained upon reprocessing as a function of temperature (from −60 °C to 110 °C), under N_2 flow, at a heating rate of 3 °C min^{-1}. Specimens with dimensions of 5.5 mm × 6 mm × 2.5 mm were used for the measurements. The tests were conducted with an oscillation amplitude of 20 μm and a frequency of 1 Hz.

A stress relaxation test in tensile mode was estimated to analyze the temperature-dependent bond exchange and the flow behavior of the NIPU films at different temperatures. Experiments were carried out at 80 °C, 100 °C and 120 °C, applying a 0.3% constant strain (TA DMA 850, TA instruments). The characteristic relaxation time (τ^*) was determined according to the Kohlrausch–Williams–Watts (KWW) model (eqn (6)), where multiple mechanisms with different relaxation times are involved.[63]

$$\frac{E(t)}{E_0} = \exp\left(-\left(\frac{t}{\tau^*}\right)^\beta\right) \quad (6)$$

where $E(t)/E_0$ is the normalized elastic relaxation modulus with respect to that at time zero, and t and τ^* are the experimental and characteristic relaxation times, respectively. The parameter β is the stretching exponent, which defines the width of the relaxation time distribution in the system. $\beta = 1$ indicates that the system has a single relaxation time following the single-mode Maxwell model,[64,65] whereas $\beta < 1$ suggests a broad distribution of relaxation times.[66] The average relaxation time $\langle\tau\rangle$ for the stretched exponential model was calculated using eqn (7).

$$\langle\tau\rangle = \int_0^\infty \exp\left(-\left(\frac{t}{\tau^*}\right)^\beta\right)dt = \frac{\tau^* \Gamma\left(\frac{1}{\beta}\right)}{\beta} \quad (7)$$

where Γ is the Gamma function.

The activation energy was calculated by fitting the experimental data with the Arrhenius equation (eqn (8)):

$$\ln\langle\tau\rangle = \ln(\tau_0) + \frac{E_a}{R}\left(\frac{1000}{T}\right) \quad (8)$$

where τ_0 (s) is the relaxation time at zero time, E_a (kJ mol^{-1}) is the activation energy, R is the ideal gas constant (J mol^{-1} K) and T is the temperature (K).

2.6.6 Gel content. The gel content (GC) of NIPU foams and reprocessed films was estimated according to the procedure available in the open literature.[44,63] Approximately 30 mg of sample were weighted (w_i) and immersed in 30 mL THF for 24 h. Subsequently, the samples were dried in an oven at 70 °C for 24 h and weighed again (w_{dry}). GC was calculated according to eqn (9).

$$GC = \frac{w_{dry}}{w_i} \times 100 \quad (9)$$

3. Results and discussion

3.1 Synthesis and characterization of CSBO

The conversion of ESBO and the yield of CSBO were measured by quantitative ^{1}H-NMR from the disappearance of the epoxy peaks in the region 2.8–3.2 ppm and the appearance of carbonated peaks at 4.2–5 ppm (Fig. 2a). Complete conversion of ESBO and 90% yield of CSBO were obtained after 24 h of reaction (Fig. S2, Section S2, SI), comparable with other works.[25] The formation of keto by-products was also observed in the spectra at 2.4 ppm, in agreement with the work of Natongchai *et al.*[67] The starting epoxy ESBO is a complex mixture of triglycerides with different fatty acid compositions (Table S1, Section S2, SI). Considering the CSBO yield and the ESBO composition, the CSBO average functionality was 3.7. FTIR analysis of the starting material and final reaction product confirmed the full conversion of ESBO by the

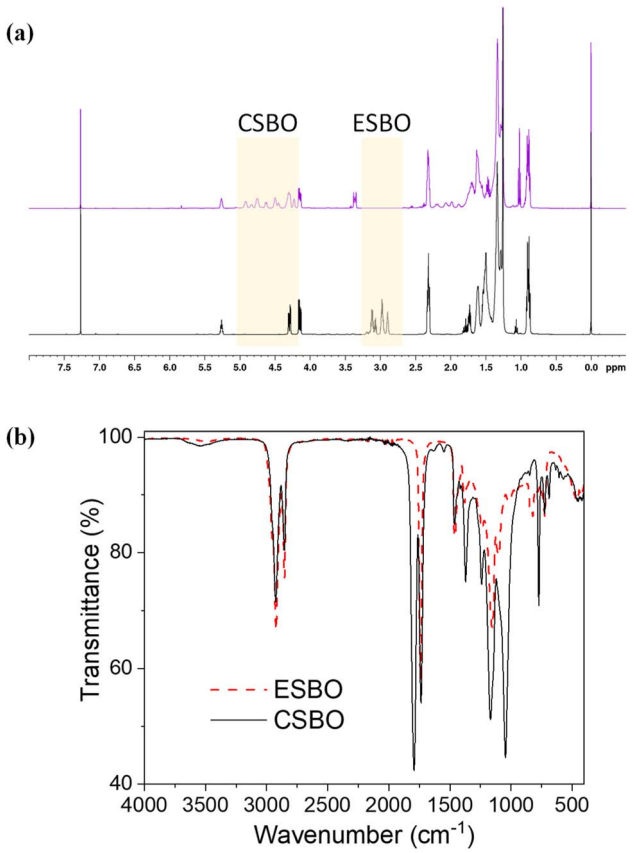

Fig. 2 (a) ^{1}H-NMR spectra of ESBO (black line) and the reaction product after a 24 h-carbonation experiment prior to purification from the catalyst (purple line); (b) FTIR spectra of ESBO and CSBO within the wavenumber range of 4000–500 cm^{-1}.

disappearance of the signal in the region 815–950 cm^{-1} (C–O–C stretching of oxiranes) and the appearance of the band at 1800 cm^{-1} (Fig. 2b).[49,68,69] The thermo-degradative behavior of the synthesized CSBO was also investigated and reported in Table S2 (Section S3, SI). FTIR spectra of CSBO and precursors are reported in Fig. S3 (Section S2, SI) and commented on in Section S2.

3.2 *S*-Alkylation experiments

The occurrence of *S*-alkylation of CSBO was verified by conducting dedicated experiments with DODT and both CSBO and the blend CSBO/BCC, as described in Section 2.5. Samples were collected from the reaction solutions every 20 min and analyzed through ATR-FTIR spectroscopy. The conversion of CC groups was determined quantitatively by integrating the peak at 1800 cm^{-1}, according to eqn (1) and (2). When DODT and CSBO were employed, no significant variations over time were registered (Fig. 3). Moreover, the peak at 3500 cm^{-1} related to the hydroxyl groups of the hydroxythioether linkage[27] was not observed and simultaneously the peak at 1800 cm^{-1} related to the CC groups did not decrease over time suggesting that the *S*-alkylation did not take place within the selected reaction time. When reacting DODT with BCC, the peak of CC gradually decreased over time, reaching almost 100% conversion after 120 min (Fig. 4a and b). Additionally, a new peak at 3500 cm^{-1} appeared soon after 20 min of reaction, indicating the formation of hydroxyl groups related to the hydroxythioether linkages.

Therefore, it can be concluded that the different activities of CSBO and BCC in the *S*-alkylation reaction directly reflect their different structural properties. The chemical structure of CSBO contains only internal CCs and lacks unsubstituted methylene groups which would facilitate the nucleophilic attack by thiol

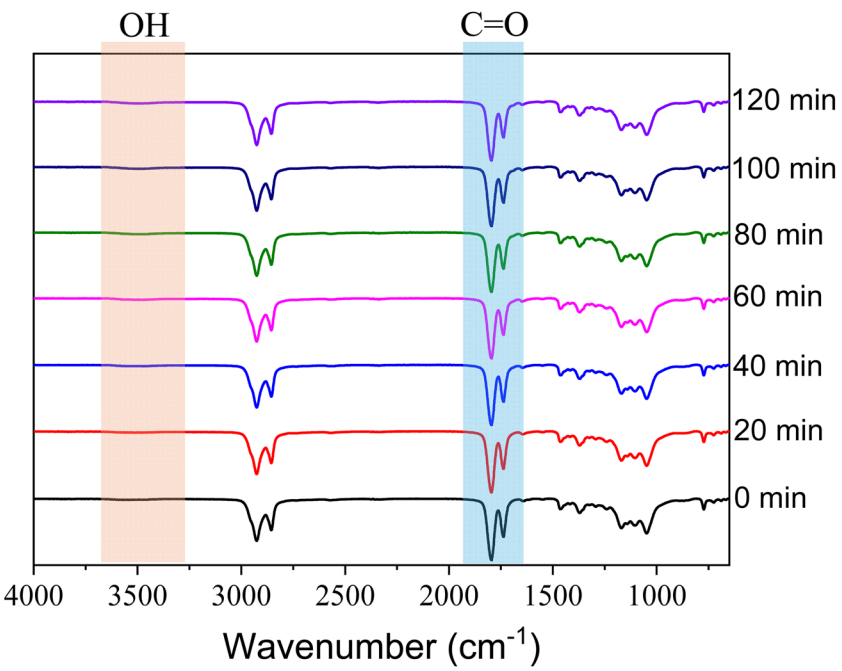

Fig. 3 FTIR spectra of the reaction solution of CSBO/DODT as a function of the reaction time. Samples were collected every 20 min and analyzed in the range of 4000–800 cm^{-1} wavenumber.

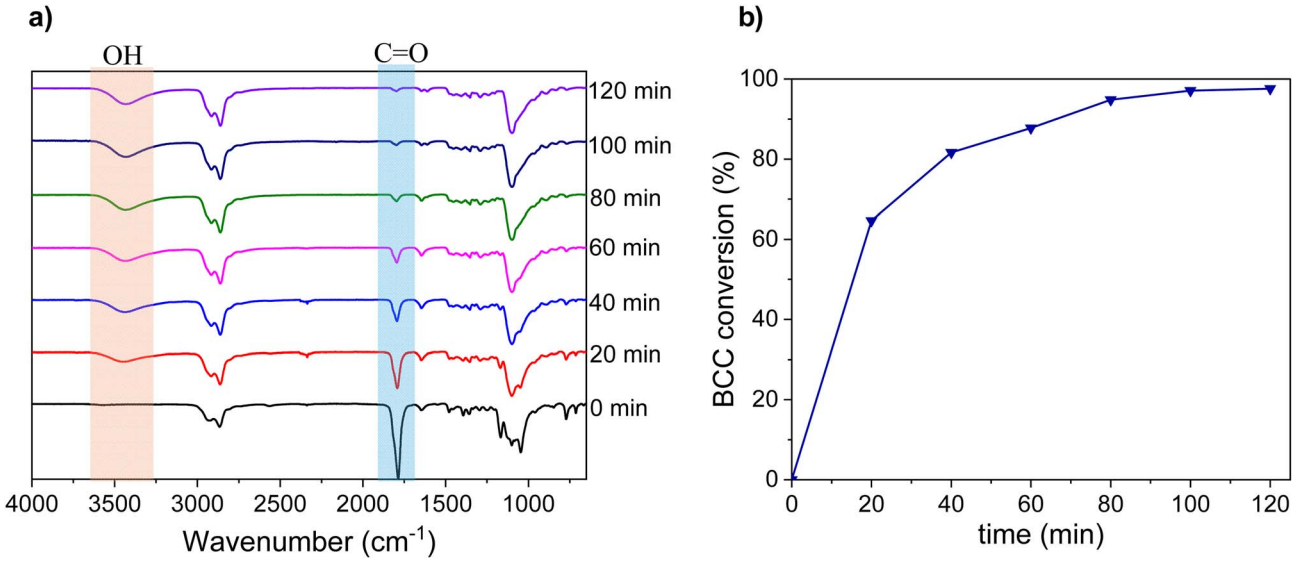

Fig. 4 (a) FTIR spectra of the reaction between BCC and DODT as a function of reaction time. (b) BCC conversion over time of reaction calculated according to eqn (1) and (2).

groups.[42,43] In contrast, BCC features two external CCs with two unsubstituted methylene groups, making it significantly more reactive with thiols in the *S*-alkylation route.

3.3 Characterization of NIPU foams

The composite foams were chemically, thermally, morphologically and mechanically characterized, as described in Section 2.6. The main physical and morphological parameters are displayed in Table 3. The apparent density of the foams ranged from 200 to 700 kg m^{-3} (Table 3). NIPU_1 containing no BCC exhibited an apparent density of 600 kg m^{-3}. As demonstrated by the experiments in Section 3.3, *S*-alkylation did not occur between CSBO and DODT; thus, foaming of NIPU_1 was solely attributed to the incorporation of air during mechanical stirring, *i.e.* frothing, leading to bubbles entrapped in the polymeric matrix.[70] To verify this, a thiol-free formulation (NIPU_2) was synthesized from CSBO and BDA, resulting in a comparable density. In contrast, when BCC was incorporated, *S*-alkylation reaction occurred producing CO_2 *in situ*, and resulting in NIPU_3 and NIPU_4 foams with significantly lower densities (200–270 kg m^{-3}), consistent with other bio-based NIPU foams reported by previous works.[27,43,63] The different foam densities were strictly correlated to the different morphologies of the foam cells (Fig. 5). NIPU_1 and NIPU_2 exhibited tiny bubbles of rounded cell morphology with respective anisotropy coefficients of 1.1 ± 0.3 and 0.9 ± 0.2, typical of frothed foams. In case of NIPU_1, the unreacted thiol reduced the overall viscosity of the polymeric mixture resulting in an increased cell density and size (Table 3).

Remarkable morphological differences were observed when employing the blends of bio-based CCs while keeping constant molar ratios of the other components (Fig. 5, NIPU_3 and NIPU_4). Irregular open cell-like morphology with an average cell size in the range of 450–650 μm was obtained, in agreement with other open-cell-like bio-based NIPU and PU composite foams.[4,11,43,45] The irregular shape of the cell structures might be associated with the difficulty in regulating the self-blowing routes due to the relatively high viscosity of the systems. In the case of NIPU_4, a higher concentration of CCs led to lower cell size distribution and increase of the cell density by 50%, probably because of the higher amount of nucleating sites.

The gel content (GC) of the NIPU foams was determined and found to be in the range 77.2–83.2% (Table 2), in agreement with previously reported bio-based NIPU foams.[43,45] The very close values between the different foams suggested a similar crosslinking degree. NIPU_2 showed a slightly higher GC value with respect to the others probably because of the higher amount of BDA, which generated higher crosslinking with CSBO. Moreover, the higher content of hydrophobic soybean oil in the formulations of NIPU_1 and NIPU_2 with respect to the other foams may result in materials that are less sensitive to hydroplasticization induced by ambient humidity, thereby contributing to the observed increase in gel content. Although NIPU foams derived from petrol-based precursors and conventional PU foams usually exhibit GC values higher than 90%,[71,72] the comparatively lower GC values herein obtained provide a beneficial balance between structural integrity and reprocessability, aligning with the design of recyclable, bio-based foamed systems.[27,48]

The chemical characterization of the foams was carried out through FTIR spectroscopy (Fig. S4, Section S4, SI). The signals at 1695 and 1535 cm^{-1}, characteristic of the NH stretching and bending vibrations, the hydroxyl groups in the wavenumber range of 3500–3000 cm^{-1}, and the carbonyl group associated with the urethane bonds at 1690 cm^{-1} (ref. 61) were identified in all spectra, confirming the formation of hydroxyurethane and hydroxythioether linkages. A small peak at 1800 cm^{-1} associated with CC groups suggested the presence of residual

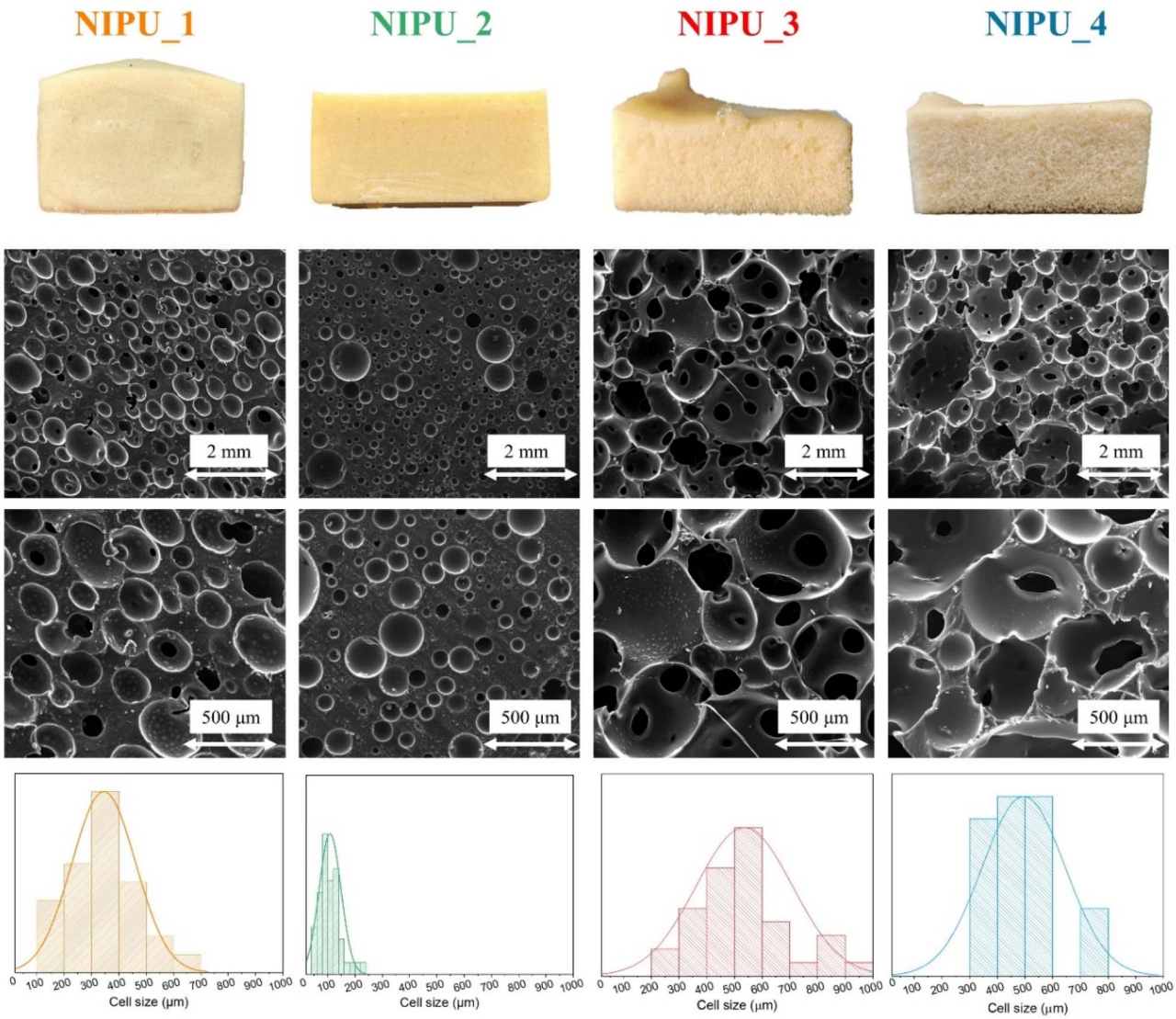

Fig. 5 Digital and Scanning Electron Microscopy (SEM) images of the selected NIPU foams. Upper: magnification 50×, scale bar = 2 mm. Middle: magnification 200×, scale bar = 500 μm. Bottom: cell size distribution of the NIPU foams. Measurements were done considering 100 cells for each sample.

unreacted cyclic carbonates, which is typical of highly viscous and sterically hindered self-blowing NIPU systems.[27,61]

The thermal properties of the foams, *i.e.*, the thermal degradation temperature at 5% weight loss ($T_{d5\%}$), the maximum degradation temperature (T_{dmax}), the residual weight at 600 °C ($w_{d600°C}$) and the glass transition temperature (T_g), are reported in Table 3.

The glass transition temperatures (T_g) determined from the second heating scan were considered representative of the thermally equilibrated materials and fall within the range reported in the literature.[43,46,71] As a matter of fact, no marked differences were observed between the first and second heating scans, indicating that no detectable post-curing reactions involving residual cyclic carbonate occurred within the

Table 2 Gel content, as well as physical, morphological, and mechanical properties of the NIPU foams. Results are expressed as the average and standard deviation of three independent measurements

Sample name	GC (%)	ρ (kg m^{-3})	D_h (μm)	$N \times 10^{-3}$ (cm^{-3})	Anisotropy coefficient (–)
NIPU_1	78.6 ± 5.2	600 ± 50	366 ± 13.3	4.4 ± 0.1	0.9 ± 0.1
NIPU_2	83.2 ± 4.3	700 ± 55	100 ± 80	0.02 ± 0.0005	1.1 ± 0.3
NIPU_3	77.2 ± 8.2	200 ± 70	535 ± 173	0.6 ± 0.03	0.9 ± 0.2
NIPU_4	78.0 ± 2.0	250 ± 10	495 ± 150	1.2 ± 0.06	0.9 ± 0.1

Table 3 Thermal properties of NIPU foams

Sample name	$T_{d5\%}$ (°C)	T_{dmax} (°C)	$w_{d600°C}$ (%)	T_g (°C)
NIPU_1	162.9	387	2.8	3.0
NIPU_2	208.4	383	1.9	5.1
NIPU_3	188.7	392	2.6	−12.7
NIPU_4	221.6	385	2.9	−14.1

investigated temperature range. Moreover, the absence of exothermic peaks during the DSC scans suggests that additional network formation during thermal analysis is negligible. The thermodegradative behaviors of all the foams are presented in Fig. 6. Two predominant stages of thermal degradation were revealed for NIPU_1 and NIPU_2 foams. The first degradation step, with an onset temperature of approximately 300 °C, was attributed to the decomposition of urethane linkages.[27] The second stage, occurring at around 435 °C, was ascribed to the breakdown of secondary products formed during the initial degradation phase, likely originating from CC-based intermediates derived from the precursors and diamine used in the NIPU synthesis.[73] Both foams also exhibited minor mass losses (<2 wt%) below 180 °C, which can be attributed to the evaporation of residual low-boiling-point components or the decomposition of the unreacted monomers.[61] Regarding the foams NIPU_3 and NIPU_4, two main degradation events were observed within the temperature range of 315–445 °C. These are associated with the decomposition of urethane and thiourethane bonds. This process generates lower-molecular-weight compounds, which undergo further degradation at around 445 °C. Minor mass losses (<2 wt%) were detected below 150–200 °C, attributed to either the volatilization of residual solvents or the removal of remaining impurities. Overall, the residual weight upon thermal degradation at 600 °C was in the range of 2–3 wt%.

The glass transition temperatures in Table 3 were retrieved from DSC curves (Fig. S5, Section S5, SI), where no melting or phase transition was observed. The highest T_g was registered in the case of NIPU_2, which contained the highest amount of diamine and no BCC in the formulation. That led to high crosslinking of the hydroxyurethane linkages and thus higher rigidity of the final material. NIPU_1 still showed a positive but slightly lower T_g compared to NIPU_2, suggesting the formation of similar rigid and compact networks. Finally, the other NIPU foams formulated by varying the CSBO/BCC ratios (NIPU_3 and NIPU_4) showed negative T_g values as introducing hydroxythioether bonds was found to decrease T_g[61] indicating the formation of flexible foams.

The results of the mechanical tests of the NIPU foams are shown in Fig. 7a. All samples can be classified as elastomeric foams, being characterized by the three typical deformation regions: (i) a linear-elastic region, where cell walls and edges bend; (ii) a plastic plateau, during which cell walls buckle, yield, or fracture; and (iii) a densification region, where the cell walls collapse and compact. In the case of NIPU_1 and NIPU_2, the plateau region was almost negligible, with an abrupt transition from the elastic to densification regime. In contrast, NIPU_3 and NIPU_4 exhibited an opposite behavior, showing a very short elastic region and a long distinct plateau. The densification region of NIPU_4 was not fully captured, as the maximum applicable load of the testing instrument (18 N) was insufficient to reach this deformation stage. The values of elastic modulus

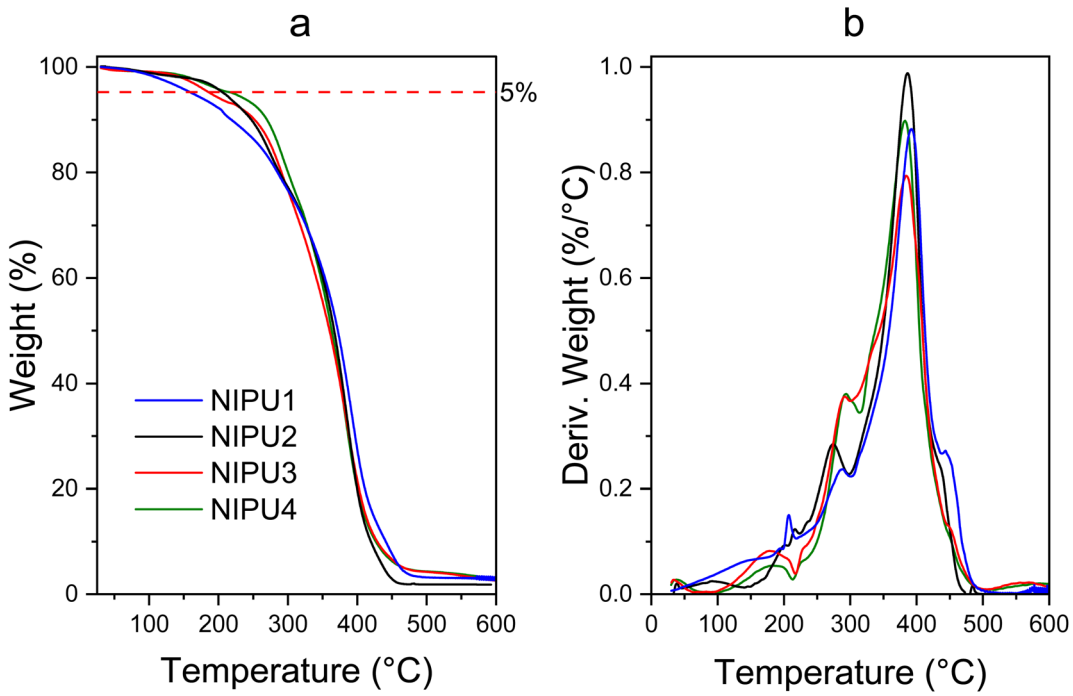

Fig. 6 Thermodegradative (a) and derivative thermodegradative (b) curves of NIPU foams.

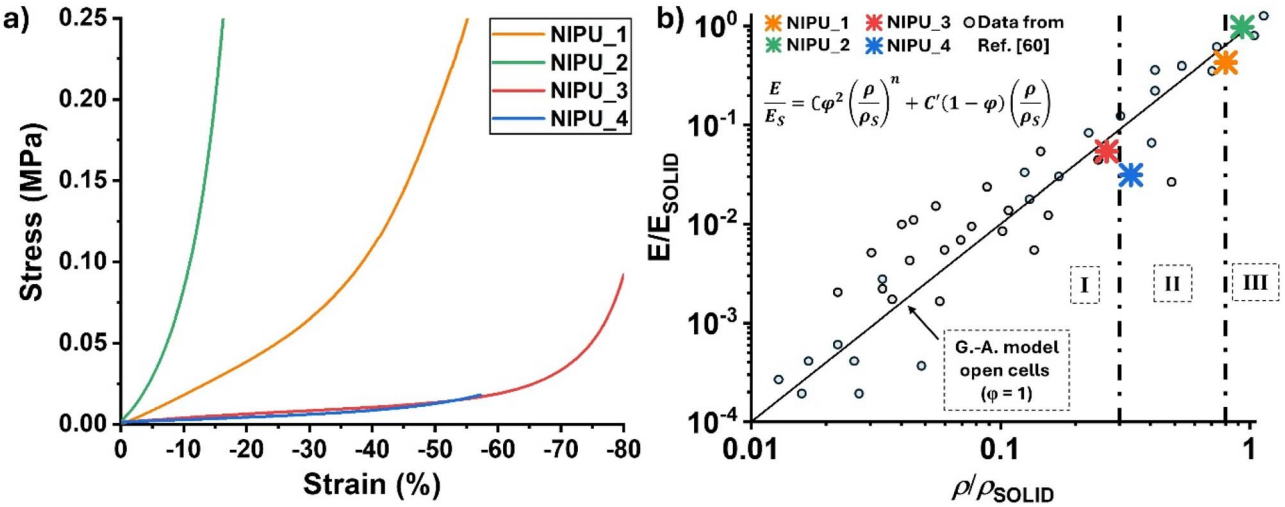

Fig. 7 (a) Compressive stress–strain curves of the examined NIPU foams. (b) Graphical representation of the Gibson–Ashby model for open-cell and closed-cell foams in correlation with the results obtained for the examined NIPU foams.[60]

(E', kPa) and compressive strength evaluated at 10% deformation (σ_{10}, kPa) are reported in Table 4. NIPU_1 and NIPU_2 showed the highest σ_{10} and E' reflecting their rigidity while NIPU_3 and NIPU_4 had the lowest values suggesting high flexibility of the materials.

To ensure a fairer comparison, the mechanical properties of the NIPU foams were normalized by their apparent densities (Table 4). By dividing σ_{10} and E' by the corresponding density, the specific strength σ^*_{10} (σ_{10}/ρ) and specific modulus E'^* (E'/ρ) are obtained. NIPU_3 and NIPU_4, obtained with different blends of CSBO and BCC but with unaltered nucleophile content (BDA and DODT, Table 1), showed comparable specific strength and modulus. On the other hand, NIPU_2, synthesized only from CSBO and BDA, showed higher specific strength and modulus values due to higher crosslinking and rigidity.

The mechanical data were analyzed using a modified Gibson–Ashby model presented in eqn (5)[6] and reported in Fig. 7b as the normalized modulus E/E_S *versus* the relative density ρ/ρ_S. For comparison, the predictions of the classical Gibson–Ashby model for ideal foams are shown as a solid line in Fig. 7b. Moreover, data of different foam systems were collected from ref. 60 and plotted as scattered points in Fig. 7b to compare the present NIPU systems with conventional ones. To calculate the relative modulus and density, the reference values for the solid material Es and ρ_S were set equal to 4.8 kPa and 750 kg m^{-3}, respectively, which were determined from compression tests on the second generation reprocessed material (Section 3.4). The values of the coefficients C and C' as well as the fitted parameters n and φ are displayed in Table 4. The n parameter gives an indication of the dominant deformation mechanism of the porous network and it usually varies between 1 (for stretching-dominated mechanisms) and 2 (for bending-dominated ones). The fitted n parameters for NIPU foams in Table 4 range between 1.4 and 1.9 indicating mixed bending-stretching behavior. This is typical of open-cell networks that retain a measurable fraction of closed-cell faces. On the other hand, the ratio φ provides insight into which structural elements of the foam predominantly carry the applied load, *i.e.*, cell edges (beams) or cell faces (walls). The distinction is relevant since edges deform mainly by elastic bending, whereas walls respond by stretching. As a result, NIPU_1 and NIPU_2 exhibited the highest φ values (0.97 and 0.96, respectively, Table 4), indicating that most of the load was supported by the edges. In contrast, NIPU_3 and NIPU_4 showed lower φ values of 0.44

Table 4 Results of mechanical tests. $\sigma_{10\%}$: compressive strength at 10% deformation, E': elastic modulus, specific compressive strength at 10% deformation-σ_{10}/ρ (σ^*_{10}) and specific elastic modulus-E'/ρ (E'^*) and the estimated parameters of the Gibson–Ashby's model of the NIPU foams

	Mechanical properties				Gibson–Ashby adapted model					
Sample name	$\sigma_{10\%}$ (kPa)	E' (kPa)	σ_{10}/ρ (σ^*_{10}) (kPa m^3 kg^{-1})	E'/ρ (E'^*) (kPa m^3 kg^{-1})	ρ/ρ_S	E/E_S	C^a	C'^b	n^c	φ^c
NIPU_1	12.9 ± 1.2	2.1 ± 0.3	0.02	0.0034	0.8	0.4	0.8	0.5	1.9	0.9
NIPU_2	83.5 ± 8.6	4.7 ± 0.5	0.2	0.0067	0.9	0.9	1.1	1.0	1.4	0.9
NIPU_3	3.9 ± 0.6	0.30 ± 0.04	0.02	0.0013	0.3	0.05	0.8	0.2	1.4	0.4
NIPU_4	2.8 ± 0.4	0.20 ± 0.03	0.01	0.0006	0.3	0.03	0.3	0.094	1.6	0.7

[a] $\varphi = 1$ and $n = 2$ in eqn (5). [b] $\varphi = 0$ in eqn (5). [c] Retrieved from eqn (5).

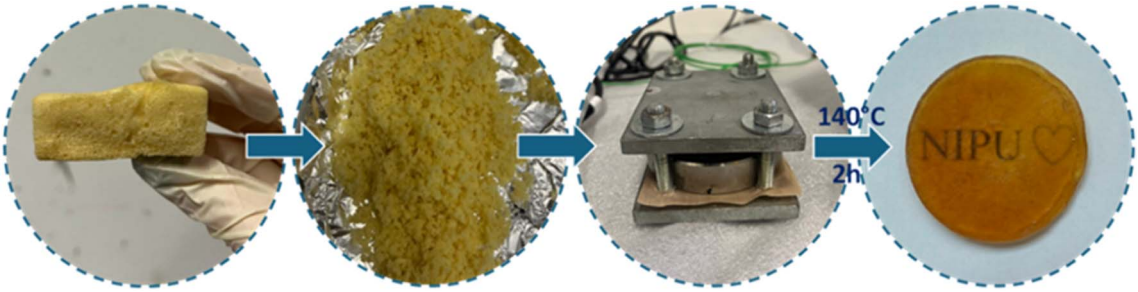

Fig. 8 Workflow for the reprocessing of NIPU foams into elastic films.

and 0.64, respectively. This suggests a more balanced load contribution between edges and walls, responding with both elastic buckling and face stretching. This is particularly evident for NIPU_3, whose optimized reactant ratio likely resulted in a more homogeneous pore architecture, with cell-wall thicknesses comparable to those of the edges.

According to Gibson and Ashby,[60] three regimes can be identified in the plot of E/E_S as a function of ρ/ρ_S depending on the ρ/ρ_S ratio. Materials with $0 < \rho/\rho_S < 0.3$ can be considered as true "foams", those with $0.8 < \rho/\rho_S < 1$ correspond to "holes in a solid", and the intermediate range ($0.3 < \rho/\rho_S < 0.8$) defines pseudo-foams with hybrid characteristics. Based on this classification, NIPU_1 and NIPU_2 are positioned in the third regime (Fig. 7b), confirming that they behave more as solids with dispersed voids than as true foams. NIPU_3 falls in the first section confirming its foam-like behavior, in agreement with the experimental observations. NIPU_4 lies near the boundary between the first and second regimes, suggesting a more hybrid morphology likely induced by the excess cyclic carbonate content with respect to that of the nucleophiles (CCs : nucleophiles = 1.1 : 1). These results align well with the SEM images presented in Fig. 5.

3.4 Reprocessing and characterization of NIPU foams

3.4.1 Chemical, thermal, and mechanical characterization. NIPU foams were successfully reprocessed *via* compression molding into thin, highly elastic, semi-transparent, crack-free and homogeneous films. Specifically, the foam with the best mechanical properties, *i.e.*, NIPU_3, was milled and reprocessed *via* compression moulding at 140 °C for 2 h (Fig. 8) into the new material NIPU_3_film. The reprocessing of NIPU foam was possible due to the presence of dynamic hydroxyurethane bonds which undergo reorganization upon exposure to elevated temperatures or mechanical stimuli.[43] In case of NIPUs synthesized from vegetable oil-derived CC and diamines, three mechanisms of dynamic bond exchanges are known, *i.e.*, reversible aminolysis, transcarbamoylation and transesterification,[35,45,74] where the former is dissociative while the latter ones are associative. In dissociative mechanisms, the degree of crosslinking of the material is temporarily reduced, as bond dissociation occurs before new bonds are created. In contrast, associative mechanisms involve simultaneous bond breaking and reforming, keeping the material's crosslinking degree essentially constant.[75–77]

The FTIR spectrum of NIPU_3_film is shown in Fig. S6 (Section S6, SI), where a comparison with that of the native foams was done. No relevant variations in the functional groups of NIPU foams were observed, except for the case of the peak at 1790 cm^{-1}, which was reduced in intensity upon reprocessing.

The GC values of the NIPU film are reported in Fig. 9 and compared with those of the native NIPU_3 foam, of an isocyanate-based flexible PU foam as well as of a thermoplastic polyurethane (TPU).

NIPU_film_3 showed a GC of approximately 60%, which was slightly higher than that of conventional TPU materials, and lower than the GCs of NIPU and PU foams which are usually in the range of 88–95%.[33,46] The lower GC of the NIPU film might be associated with a reduction in the effective crosslinking density induced by partial thermal degradation during reprocessing (as revealed also by TGA), which may generate more soluble fractions without contributing to further network formation. Moreover, T_g, determined from DSC analysis, was −15.73 °C (Fig. S7, Section S6, SI), which was close to that of the

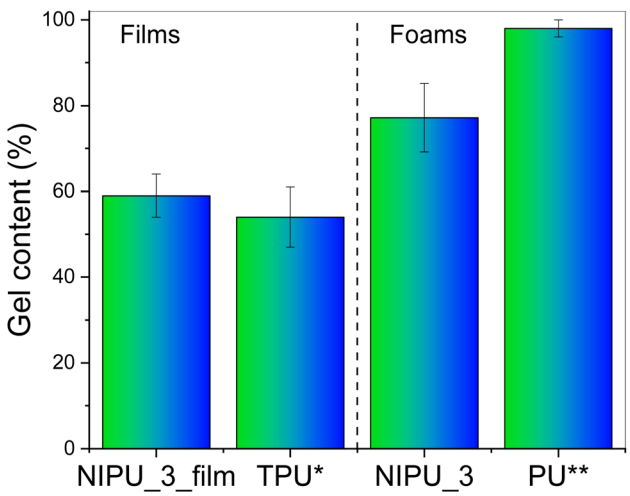

Fig. 9 Gel content of the examined systems, *i.e.*, NIPU-film_3, commercial TPU, native NIPU_3 and conventional flexible PU foam. Legend. *TPU film was obtained through melt mixing of TPU pellets at 220 °C for 5 minutes, **flexible PU foam was synthesized using conventional polyether-polyol and aliphatic isocyanate 1,5-pentanediisocyanate (PDI).

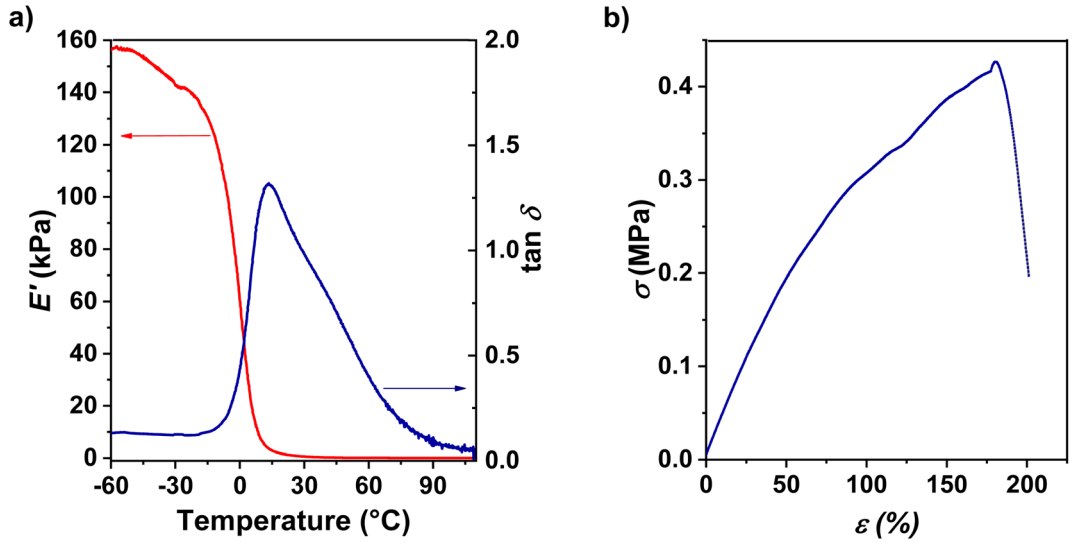

Fig. 10 NIPU_3_film mechanical characterization through tensile tests: (a) storage modulus and tan(δ) as a function of temperature. (b) Stress *vs.* elongation.

native foam. The tensile properties of NIPU_3_film are displayed in Fig. 10. The storage modulus (E') and the damping ratio ($\tan(\delta) = E'/E''$) as a function of temperature and the tensile stress *vs.* strain curve are displayed in Fig. 10a and b, respectively. The storage modulus attained the rubbery plateau at approximately 20 °C, corresponding to the achievement of the maximum value of tan(δ). The glass transition temperature (T_g'), estimated from DMA analysis as the point where the storage modulus sharply decreases (the onset of the curve drop), was found to be 0 °C, in agreement with Purwanto *et al.*[61] The tensile curve (Fig. 10b) of NIPU_3_film exhibited the typical behavior of an elastomeric material. Results were averaged among data obtained upon tests performed on five independent specimens. The elongation at break (ε) was found to be 137.9 ± 3.0%,

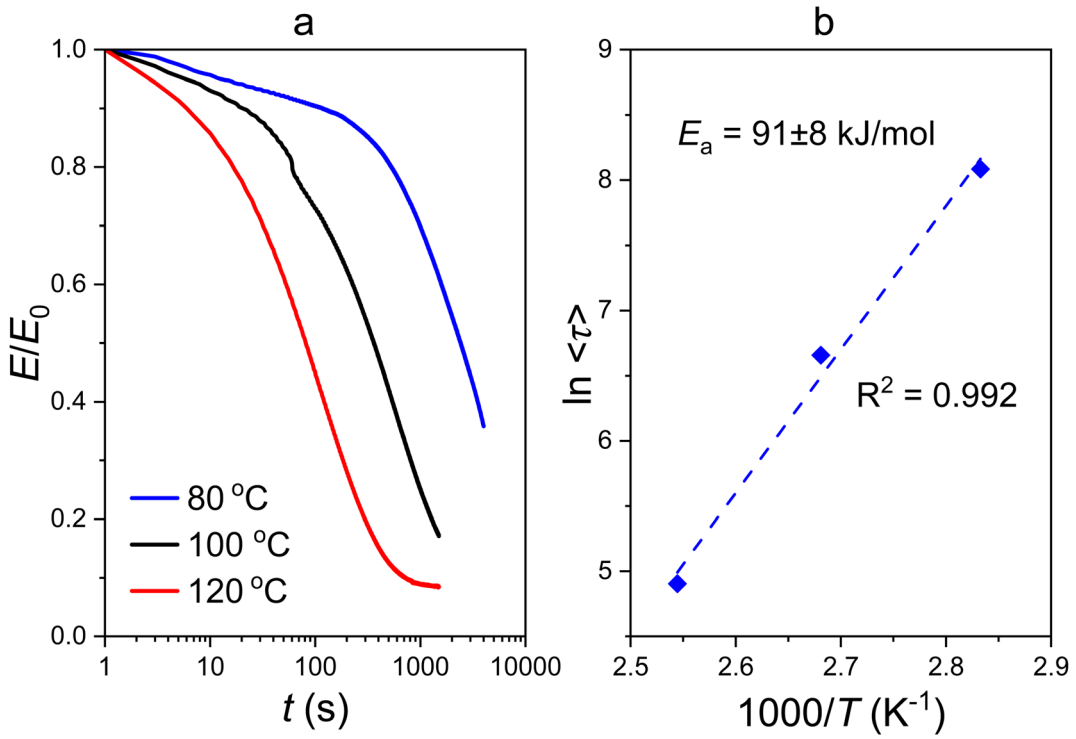

Fig. 11 (a) Normalized stress relaxation curves of the examined NIPU film (NIPU_3_film) at 80, 100, and 120 °C. (b) Arrhenius plot of the stress relaxation average time distribution.

Table 5 Fitting parameters for stress-relaxation curves based on the KWW model

Temperature (°C)	τ^* (s)	$\langle\tau\rangle$ (s)	β (–)
80	3066	3246	0.9
100	597	777	0.7
120	112	135	0.7

corresponding to the maximum strength (σ_{max}) of 0.43 ± 0.02 MPa. The elastic modulus (E) was determined as the slope of the initial linear trait of the curve, and was found to be 0.4 ± 0.05 MPa (R^2 equal to 0.999).

3.4.2 Stress-relaxation properties. The stress-relaxation behavior in tensile mode of the reprocessed material at three different temperatures, *i.e.*, 80, 100, and 120 °C, is shown in Fig. 11a. For all cases, the normalized stress relaxation modulus (E/E_o) presented a decreasing trend by increasing the relaxation time. As expected, the stress-relaxation rate increased with temperature, with the fastest decrease in relaxation modulus observed at 120 °C. The data were described according to the KWW model (eqn (6)) as an exponential decay of the relaxation modulus with time, and the parameters β and τ^* were fitted accordingly.[75,76] Finally, the average relaxation time $\langle\tau\rangle$ was retrieved according to eqn (7). The numerical values of the parameters resulting from the fitting of the stress-relaxation data and the average relaxation time $\langle\tau\rangle$ based on the KWW model are displayed in Table 5. As a result, the characteristic relaxation time τ^* and the average relaxation time $\langle\tau\rangle$ decreased with increasing temperature, since the relaxation phenomena are enhanced at higher temperatures. The parameter β, which is related to the width of the relaxation time distribution, displayed the highest value of 0.89 at 80 °C, suggesting the narrowest distribution of relaxation times due to a less complex process dominated by a single type of relaxation mechanism. At higher temperatures, *i.e.*, 100 °C and 120 °C, lower β values were registered, corresponding to a broader relaxation time distribution and suggesting an increased complexity of the relaxation mechanisms, such as covalent bond exchange.[77]

The apparent activation energy E_a was determined from the slope of the Arrhenius plot (Fig. 11b), according to eqn (8), and was found to be 91 ± 8 kJ mol^{-1} (R^2 equal to 0.992). This value is consistent with the E_a values reported in the open literature for NIPU foams prepared with bi-functional thiol cross-linkers, and indicates that the relaxation mechanisms within the NIPU networks have a relatively strong temperature dependence.[61,77] This relies on the fact that stress relaxation in dynamic polymer networks is influenced by a combination of the material's viscoelastic properties and the energy barriers involved in the reversible chemical reactions that define the dynamics of the network.[76]

Further investigations will focus on exploring the effect of relevant reprocessability parameters such as temperature, pressure and time of the compression moulding, as well as the possibility of using multiple reprocessing steps on the dynamic bond mechanisms. Moreover, the more challenging foam-to-foam (refoaming) process will also be investigated in the future, aligning with the circular economy principles.

4. Conclusions

Self-blowing bio-based non-isocyanate polyurethane (NIPU) foams were successfully synthesized for the first time using blends of bio-based cyclic carbonates composed by carbonated soybean oil (CSBO) and bio-derived butanediol bis-cyclocarbonate (BCC). CSBO was synthesized *via* CO_2 cycloaddition to epoxidized soybean oil (ESBO), achieving 90% yield after 24 h. The dynamics of the *S*-alkylation of the CCs with 3,6-dioxa-1,8-octanedithiol (DODT) was investigated revealing that BCC actively underwent decarboxylation by DODT, as evidenced by the disappearance of the cyclic carbonate absorption band at 1790 cm^{-1} within 2 h. In contrast, CSBO showed no reactivity in the *S*-alkylation reaction under the selected operating conditions, as its FTIR spectral features remained unchanged with the reaction time. These results indicate that terminal unsubstituted methylene groups in the CC structures are essential for enabling nucleophilic attack by thiols required to produce self-blowing NIPU foams. Different formulations of NIPU foams were prepared and characterized by chemical, thermal, morphological, and mechanical analyses. Among the selected formulations, the CSBO/BCC blend yielded foams with the most promising properties, having the lowest densities (190–250 kg m^{-3}) and bio-based content of 92%. Mechanical evaluation using a modified Gibson–Ashby model revealed that different formulations fell into distinct material categories, ranging from "holes-in-solid" (NIPU_1 and NIPU_2) to pseudo-foams (NIPU_4) and full foams (NIPU_3). These distinctions were quantified by the φ parameter, representing the structural part of the foam bearing the mechanical load. Notably, NIPU_3 exhibited the lowest φ value, indicating a more balanced stress distribution between foam edges and walls. Finally, the foams were successfully reshaped into semi-transparent flexible films under temperature-controlled compression molding, demonstrating their recyclability and potential for new applications. Relaxation dynamics of the reprocessed material with the Kohlrausch–Williams–Watts (KWW) function and Arrhenius equation revealed a strong temperature dependence shifting from simple relaxation mechanisms at 80 °C to more complex ones at 120 °C.

In conclusion, this work broadens the understanding of the sustainable design of bio-based composites and fully reprocessable NIPU foams starting from bio-based cyclic carbonate blends, paving the way for their use as alternatives to conventional PU flexible foams.

Conflicts of interest

There are no conflicts to declare.

Abbreviations

ATR Attenuated total reflectance

BA	Blowing agent
BCC	Butanediol bis-cyclocarbonate
BDA	1,4-Butane diamine
CAN	Covalent adaptable network
CC	Cyclic carbonate
CMR	Carcinogenic, mutagenic and toxic for reproduction
CSBO	Carbonated soybean oil
DBU	1,8-Diazabicyclo(5.4.0)undec-7-ene
DMA	Dynamic mechanical analysis
DODT	3,6-Dioxa-1,8-octanedithiol
DSC	Differential scanning calorimetry
DTGA	Derivative thermogravimetric analysis
ESBO	Epoxidized soybean oil
FTIR	Fourier-transform infrared spectroscopy
GC	Gel content
GC-MS	Gas chromatography-mass spectroscopy
^{1}H NMR	Protonic nuclear magnetic resonance
KWW	Kohlrausch–Williams–Watts
NIPHU	Non-isocyanate polyhydroxyurethane
NIPTU	Non-isocyanate polythiourethane
NIPU	Non-isocyanate-polyurethane
PHU	Polyhydroxyurethane
PDI	1,5-Pentanediisocyanate
PU	Polyurethane
SEM	Scanning electron microscopy
SI	Supplementary information
TBAB	Tetrabutylammonium bromide
TGA	Thermogravimetric analysis
THF	Tetrahydrofuran
TPU	Thermoplastic polyurethane

Symbols

A	Area of acquired SEM image
$A_{CC,t}$	Area of FTIR peak related to CC groups at time t
A_{ref}	Area of FTIR peak taken as the reference
C, C'	Proportional constants of the Gibson–Ashby model
D_h	Average cell size
E	Tensile elastic modulus
E_a	Activation energy
E_s	Modulus at material constituting the walls and the edges of the pores
E_o	Modulus at time zero
E'	Storage modulus
E''	Loss modulus
f	Functionality
M_w	Molecular weight
N	Cell density
n	Number of cells
R	Ideal gas constant
$R_{CC,t}$	Ratio of FTIR peak area related to CC to that of the reference at time t
R_{CC,t_0}	Ratio of FTIR peak area related to CC to that of the reference at time t_0
$\tan\delta$	Damping ratio
T	Temperature
$T_{d5\%}$	Thermal degradation temperature at 5% weight loss
T_g	Glass transition temperature
w_{dry}	Dried sample weight
w_i	Initial weight of sample
w_{tot}	Total weight of foam
β	Stretching exponent
ε	Elongation at break
ε_{max}	Elongation at break at maximum strength value
Γ	Gamma function
ρ	Foam density
ρ_S	Density of the bulk material constituting the foam
φ	Volume of the pores constituting the foams
σ_{max}	Maximum tensile strength
σ_{10}	Strength at 10% deformation
σ^*_{10}	Specific strength at 10% deformation
τ^0	Relaxation time at zero time
τ^*	Characteristic relaxation time
$\langle\tau\rangle$	Average relaxation time

Data availability

Data will be made available on request.

Supplementary information (SI): S1: experimental conditions used to synthesize CSBO; S2: characterization of the epoxidized soybean oil; S3: characterization of the precursors; S4: FTIR of the NIPU foams; S5 DSC curves of the NIPU foams. See DOI: https://doi.org/10.1039/d5su00946d.

Acknowledgements

This study was carried out within the Made in Italy-Circular and Sustainable Extended Partnership (MICS) and received funding from the European Union Next-Generation EU (Piano Nazionale di Ripresa e Resilienza (PNRR)-missione 4 componente 2, investimento 1.3-D. D. 1551.11-10-2022, PE00000004) and Horizon EU project INTEGRANO-G.A. 101138414 (title: Multi-dimensional integrated 623 quantitative approach to assess safety and sustainability of nanomaterials in real case life cycle scenarios using nanospecific impact categories). The work is also part of the activities financed by the Academy of Finland through the Academy Professor grants 319002, 320115, and 345053 (Prof. Tapio Salmi, Federica Orabona). Financing from Åbo Akademi University Graduate School (Federica Orabona) is gratefully acknowledged. The Walter Ahlström foundation is gratefully acknowledged for the financial support (Federica Orabona). The authors wish to thank Marco Fiume (IPCB-CNR) for the design of the graphical abstract and Mrs Alessandra Aldi, Mrs Maria Rosaria Marcedula, Mr Fabio Docimo and Mr Mario De Angioletti (IPCB-CNR) for their experimental support.

References

1 N. V. Gama, A. Ferreira and A. Barros-Timmons, *Materials*, 2023, **11**(10), 1841, DOI: 10.3390/ma11101841.
2 A. Piotrowska, J. Paciorek-Sadowska, M. Łazarska, M. Borowicz and M. Isbrandt, *Eur. Polym. J.*, 2025, **234**, 114028, DOI: 10.1016/j.eurpolymj.2025.114028.
3 Industry Data Flexible Pu Slabstock Foam, 2024, https://europur.org/flexible-pu-foam/elementor-4539, accessed on 19 th December 2024.

4 L. Verdolotti, M. R. Di Caprio, M. Lavorgna and G. G. Buonocore, Polyurethane nanocomposite foams: Correlation between nanofillers, porous morphology, and structural and functional properties, Chapter 9, *Polyurethane Polymers*, Elsevier Ltd, 2017, pp. 277–310, DOI: 10.1016/B978-0-12-804065-2.00009-7M.
5 M. Ates, S. Karadag, A. A. Eker and B. Eker, *Polym. Int.*, 2022, **71**, 1157–1163, DOI: 10.1002/pi.6441.
6 A. Demharter, *Cryogenics*, 1998, **38**, 113–117, DOI: 10.1016/S0011-2275(97)00120-3.
7 Y. Fu, C. Qiu, L. Ni, H. Ye, H. Zou, Y. Luo and M. Liang, *Constr. Build. Mater.*, 2024, **447**, 138068, DOI: 10.1016/j.conbuildmat.2024.138068.
8 N. Mahmood, Z. Yuan, J. Schmidt and C. Xu, *Renewable Sustainable Energy Rev.*, 2016, **60**, 317–329, DOI: 10.1016/j.rser.2016.01.037.
9 A. Pascarella, F. Recupido, G. C. Lama, L. Sorrentino, A. Campanile, B. Liguori, M. Berthet, G. Rollo, M. Lavorgna and L. Verdolotti, *Adv. Eng. Mater.*, 2024, **26**(8), 2301888, DOI: 10.1002/adem.202301888.
10 D. Wu, Q. Zhang, M. Hou, R. Yan, H. Lei, X. Zhou, G. Du, A. Pizzi and X. Xi, *Int. J. Biol. Macromol.*, 2024, **282**, 136892, DOI: 10.1016/j.ijbiomac.2024.136892.
11 S. Silvano, M. Moimare, L. Gryshchuk, E. Barak-Kulbak, F. Recupido, G. C. Lama, L. Boggioni and L. Verdolotti, *Int. J. Biol. Macromol.*, 2024, **278**, 135282, DOI: 10.1016/j.ijbiomac.2024.135282.
12 M. H. Karol and J. A. Kramarik, *Toxicol. Lett.*, 1196, **89**, 139–146, DOI: 10.1016/S0378-4274(96)03798-8.
13 European Commission, REACH Regulation, 2020, https://environment.ec.europa.eu/topics/chemicals/reach-regulation_en, accessed 15 th September 2024.
14 H. Blatmann, M. Fleischer, M. Bähr and R. Mülhaupt, *Macromol. Rapid Commun.*, 2014, **35**, 1238–1254, DOI: 10.1002/marc.201400209.
15 A. Cornille, S. Dworakowska, D. Bogdal, B. Boutevin and S. Caillol, *Eur. Polym. J.*, 2015, **66**, 129–138, DOI: 10.1016/j.eurpolymj.2015.01.034.
16 A. Mouren and L. Avérous, *Chem. Soc. Rev.*, 2023, **52**, 277, DOI: 10.1039/d2cs00509c.
17 A. Delaverde, G. Savin, P. Derkenne, M. Boursier, R. Morales-Cerrada, B. Nottelet, J. Pinaud and S. Caillol, *Prog. Polym. Sci.*, 2024, **151**, 101805, DOI: 10.1016/j.progpolymsci.2024.101805.
18 F. Orabona, F. Recupido, G. C. Lama, K. Polaczek, F. Taddeo, T. Salmi, M. Di Serio, L. Verdolotti and V. Russo, Cutting-edge development of non-isocyanate polyurethane (NIPU) foams: from sustainable precursors to environmental impact evaluation, *Green Chem.*, 2025, **27**, 7403–7444, DOI: 10.1039/D4GC05796A.
19 M. Ghasemlou, F. Daver, E. P. Ivanova and B. Adhikari, *Eur. Polym. J.*, 2019, **118**, 668–684, DOI: 10.1016/j.eurpolymj.2019.06.032.
20 R. Turnaturi, C. Zagni, V. Patamia, V. Barbera, G. Foresta and A. Rescifina, *Green Chem.*, 2023, **25**, 9574–9602, DOI: 10.1039/D3GC02796A.
21 W. Y. Pérez-Sena, X. Cai, N. Kebir, L. Vernières-Hassimi, C. Serra, T. Salmi and S. Leveneur, *Chem. Eng. J.*, 2018, **346**, 271–280, DOI: 10.1016/j.cej.2018.04.028.
22 P. Pescarmona, Cyclic carbonates synthesised from CO_2: Applications, challenges and recent research, trends, Current Op, *Green Sustainable Chem.*, 2012, **29**, 100457, DOI: 10.1016/j.cogsc.2021.100457.
23 M. Alves, B. Grignard, S. Gennen, C. Detembleur, C. Jerome and T. Tassaing, *RSC Adv.*, 2015, **5**, 53629–53636, DOI: 10.1039/C5RA10190E.
24 E. J. C. Lopes, A. P. C. Ribeiro and L. M. R. S. Martins, *Catalysis*, 2020, **10**(5), 479, DOI: 10.3390/catal10050479.
25 D. Kielkiewicz, A. Siewniak, R. Giada, M. Grief and A. Chrobok, *Molecules*, 2024, **229**(16), 3908, DOI: 10.3390/molecules29163908.
26 T. Cai, J. Liu, H. Cao and C. Cui, *Ind. Crops Prod.*, 2020, **145**, 112155, DOI: 10.1016/j.indcrop.2020.112155.
27 T. Wang, H. Deng, H. Zheng, J. Shen, F. Xie and C. Zhang, *ACS Sustainable Resour. Manage.*, 2024, **1**(3), 462–470, DOI: 10.1021/acssusresmgt.3c00103.
28 M. Rayung, N. Abd Ghani and N. Hasanudin, *RSC Adv.*, 2024, **14**, 9273–9299, DOI: 10.1039/D3RA08684D.
29 C. Carrè, Y. Ecochard, S. Caillol and L. Avérous, *ChemSusChem*, 2019, **12**(15), 3410–3430, DOI: 10.1002/cssc.201900737.
30 F. Orabona, S. Napolitano, V. D. Badazhkova, W. Perez-Sena, K. Eränen, R. Tesser, M. Di Serio, V. Russo and T. Salmi, *Chem. Eng. J.*, 2025, **523**, 168292, DOI: 10.1016/j.cej.2025.168292.
31 J. H. Clark, T. J. Farmer, I. D. V. Ingram, Y. Lie and M. North, *Eur. J. Org Chem.*, 2018, **31**, 4265–4271, DOI: 10.1002/ejoc.201800665.
32 X. Wang, S. Gao, J. Wang, S. Xu, H. Li, K. Chen and P. Ouyang, *Chin. J. Chem. Eng.*, 2021, **30**, 4–13, DOI: 10.1016/j.cjche.2020.12.009.
33 F. C. Destaso, C. Libretti, C. Le Coz, E. Grau, H. Cramail and M. A. R. Meier, *Green Chem.*, 2025, **27**, 4, DOI: 10.1039/D4GC05645K.
34 F. Monie, B. Grignard and C. Detrembleur, *ACS Macro Lett.*, 2022, **11**(2), 236–242, DOI: 10.1021/acsmacrolett.1c00793.
35 A. F. Guzmán Agudelo, W. J. Pérez-Sena, N. Kebir, T. Salmi, L. A. Ríos and S. Leveneur, *Chem. Eng. Sci.*, 2020, **228**, 115954, DOI: 10.1016/j.ces.2020.115954.
36 A. Cornille, C. Guillet, S. Benyahya, C. Negrell, B. Boutevin and S. Caillol, *Eur. Polym. J.*, 2016, **84**, 873–888, DOI: 10.1016/j.eurpolymj.2016.05.032.
37 O. Lamarzelle, G. Hibert, S. Lecommandoux, E. Grau and H. Cramail, *Polym. Chem.*, 2017, **8**, 3438–3447, DOI: 10.1039/C7PY00556C.
38 H. Blattmann, M. Lauth and R. Mülhaupt, *Macromol. Mater. Eng.*, 2016, **301**(8), 944–952, DOI: 10.1002/mame.201600141.
39 B. Grignard, J. M. Thomassin, S. Gennen, L. Poussard, L. Bonnaud, J. M. Raquez, P. Dubois, M. P. Tran, C. B. Park, C. Jerome and C. Detrembleur, *Green Chem.*, 2016, **8**, 2206–2215, DOI: 10.1039/C5GC02723C.

40 C. Amezúa-Arranz, M. Santiago-Calvo and M. A. Rodríguez-Pérez, *Eur. Polym. J.*, 2023, **197**, 112366, DOI: 10.1016/j.eurpolymj.2023.112366.
41 J. Sternberg and S. Pilla, *Green Chem.*, 2020, **22**, 6922–6935, DOI: 10.1039/D0GC01659D.
42 F. Monie, B. Grignard, J. Thomassin, R. Mereau, T. Tassaing, C. Jerome and C. Detrembleur, *Angew. Chem.*, 2020, **59**, 17033–17041, DOI: 10.1002/ange.202006267.
43 N. S. Purwanto, Y. Chen and J. M. Torkelson, *ACS Appl. Polym. Mater.*, 2023, **5**(8), 6651–6661, DOI: 10.1021/acsapm.3c01196.
44 M. Chaib, S. El Khezraji, S. Thakur, H. Ben Youcef, M. Lahcini and R. Verdejo, *React. Funct. Polym.*, 2024, **200**, 105924, DOI: 10.1016/j.reactfunctpolym.2024.105924.
45 D. Trojanowska, F. Monie, G. Perotto, A. Athanassiou, B. Grignard, E. Grau, T. Vidil, H. Cramail and C. Detrembleur, *Green Chem.*, 2024, **26**, 8383–8394, DOI: 10.1039/D4GC01547A.
46 Y. Chen, N. S. Purwanto, B. Chen, T. Wang, S. Kim, Y. W. Huang, W. R. Detchel and J. M. Torkelson, *Chem. Eng. J.*, 2024, **496**, 154035, DOI: 10.1016/j.cej.2024.154035.
47 M. Bourguignon, B. Grignard and C. Detrembleur, *Angew. Chem.*, 2022, **61**, 51, DOI: 10.1002/anie.202213422.
48 C. H. Tran, J. H. Park, S. Y. Lee, B. Han, W. S. Jae, H. S. Lee, H. J. Paik and I. Kim, *Polymer*, 2025, **323**, 128217, DOI: 10.1016/j.polymer.2025.128217.
49 A. Centeno-Pedrazo, J. Perez-Arce, Z. Freixa, P. Ortiz and E. J. Garcia-Suarez, *Prog. Org. Coat.*, 2024, **197**, 108830, DOI: 10.1016/j.porgcoat.2024.108830.
50 J. D. Bhaliya, S. N. Raju Kutcherlapati, N. Dhore, N. Punugupati, K. L. Sunkara, S. Misra and S. Shailesh Kumar Joshi, *RSC Sustainability*, 2025, **3**, 1434–1447, DOI: 10.1039/D4SU00587B.
51 X. Yang, C. Ren, X. Liu, P. Sun, X. Xu, H. Liu, M. Shen, S. Shang and Z. Song, *Mater. Chem. Front.*, 2021, **5**, 6160–6170, DOI: 10.1039/D1QM00765C.
52 F. Camara, S. Benyahya, V. Besse, G. Boutevin, R. Auvergne, B. Boutevin and S. Caillol, *Eur. Polym. J.*, 2014, **55**, 17–26, DOI: 10.1016/j.eurpolymj.2014.03.011.
53 M. Martínez de Sarasa Buchaca, F. de la Cruz-Martínez, E. Francés-Poveda, J. Fernández-Baeza, L. F. Sánchez-Barba, A. Garcés, J. A. Castro-Osma and A. Lara-Sánchez, *Polymers*, 2022, **14**(13), 2719, DOI: 10.3390/polym14132719.
54 N. Silmi, P. A. Dalimunthe, I. P. Mahendra, S. Purwajanti, Purwoko, R. P. Saputra, V. Suendo, Hidayat and A. A. Septevani, *Sustainable Mater. Technol.*, 2025, **45**, e01545, DOI: 10.1016/j.susmat.2025.e01545.
55 B. Galzerano, I. Capasso, L. Verdolotti, M. Lavorgna, P. Vollaro, D. Caputo, S. Iannace and B. Liguori, *Mater. Des.*, 2018, **145**, 196–204, DOI: 10.1016/j.matdes.2018.02.063.
56 F. Recupido, G. C. Lama, S. Steffen, C. Dreyer, H. Seidlitz, V. Russo, M. Lavorgna, F. De Luca Bossa, S. Silvano, L. Boggioni and L. Verdolotti, *Ecotoxicol. Environ. Saf.*, 2024, **269**, 115758, DOI: 10.1016/j.ecoenv.2023.115758.
57 W. Y. Perez-Sena, K. Eränen, N. Kumar, L. Estel, S. Leveneur and T. Salmi, *J. CO_2 Util.*, 2022, **57**, 101879, DOI: 10.1016/j.jcou.2021.101879.
58 R. R. Jay, *Anal. Chem.*, 1964, **36**(3), 667–668, DOI: 10.1021/ac60209a037.
59 R. J. Pearson, *Science*, 1966, **151**(3707), 172–177, DOI: 10.1126/science.151.3707.172.
60 I. J. Gibson and M. F. Ashby, The mechanics of three-dimensional cellular materials, *Proc. R. Soc. London, Ser. A*, 1982, **382**(1782), 43–59, DOI: 10.1098/rspa.1982.0088.
61 N. S. Purwanto, Y. Chen, T. Wang and J. M. Torkelson, *Polymer*, 2023, **272**, 125858, DOI: 10.1016/j.polymer.2023.125858.
62 F. Coccia, L. Gryshchuk, P. Moimare, F. De Luca Bossa, C. Santillo, E. Barak-Kulbak, L. Verdolotti, L. Boggioni and G. C. Lama, *Polymers*, 2021, **13**(15), 2556, DOI: 10.3390/polym13152556.
63 N. S. Purwanto, Y. Chen and J. M. Torkelson, *Eur. Polym. J.*, 2024, **206**, 112775, DOI: 10.1016/j.eurpolymj.2024.112775.
64 R. G. Ricarte and S. A. Shanbhag, *Polym. Chem.*, 2024, **15**, 815–846, DOI: 10.1039/d3py01367Gr.
65 H. Alzubi, O. Konuray, X. Fernández-Francos, X. Ramis and S. Moradi, *React. Funct. Polym.*, 2024, **196**, 105835, DOI: 10.1016/j.reactfunctpolym.2024.105835.
66 J. Lyu, S. Lee, H. Eun Bae, H. Jung, Y. II Park, Y. J. Jin, J. E. Jeong and J. C. Kilm, *Angew. Chem., Int. Ed.*, 2024, **63**, 43, DOI: 10.1002/anie.202411397.
67 W. Natongchai, S. Pornprapom and V. D'Elia, *Asian J. Org. Chem.*, 2020, **9**(5), 801–810, DOI: 10.1002/ajoc.202000154.
68 J. Li, X. Li, X. Yang, X. Xu, H. Liu and M. Zhou, *Ind. Crops Prod.*, 2023, **200**, 116842, DOI: 10.1016/j.indcrop.2023.116842.
69 P. Patel, F. Martins de Souza and R. K. Gupta, *ACS Omega*, 2024, **9**, 5862–5875, DOI: 10.1021/acsomega.3c09185.
70 R. D. Duffy, *US Pat.*, US5604267A, 1997.
71 M. Bourguignon, B. Grignard and C. Detrembleur, *Polym. Chem.*, 2025, **16**, 192, DOI: 10.1039/d4py00971a.
72 O. Gotkiewicz, M. Kirplus, Z. Walterová, O. Kočková, S. Abbrent, P. Parcheta-Szwindowska, U. Cabulis and H. Beneš, *ACS Sustainable Chem. Eng.*, 2024, **12**(4), 1605–1615, DOI: 10.1021/acssuschemeng.3c06924.
73 A. Bukowczan, P. Stachak, I. Łukaszewska, T. M. Majka, E. Hebda and K. Pielichowski, *Thermochim. Acta*, 2023, **273**, 179484, DOI: 10.1016/j.tca.2023.179484.
74 S. Hu, X. Chen and J. M. Torkelson, *ACS Sustainable Chem. Eng.*, 2019, **7**, 10025–10034, DOI: 10.1021/acssuschemeng.9b01239.
75 B. R. Elling and W. R. Ditchel, *ACS Cent. Sci.*, 2020, **6**(9), 1488–1496, DOI: 10.1021/acscentsci.0c00567.
76 D. Berne, S. Laviéville, E. Leclerc, S. Caillol, V. Ladmiral and C. Bakkali-Hassani, *ACS Polym. Au*, 2025, **5**, 214–240, DOI: 10.1021/acspolymersau.5c00004.
77 V. D. Lechuga-Islas, E. Gillissen, M. Bourguignon, B. Grignard and C. Detrembleur, *Chem. Eng. J.*, 2025, **516**, 163998, DOI: 10.1016/j.cej.2025.163998.